10.1098/rsta.2004.1451

Raman spectroscopy of diamond and doped diamond

By Steven Prawer[1] and Robert J. Nemanich[2]

[1]*School of Physics, University of Melbourne, Parkville, Victoria 3010, Australia* (s.prawer@unimelb.edu.au)
[2]*Department of Physics, North Carolina State University, Raleigh, NC 27695-8202, USA* (robert_nemanich@ncsu.edu)

Published online 29 September 2004

The optimization of diamond films as valuable engineering materials for a wide variety of applications has required the development of robust methods for their characterization. Of the many methods used, Raman microscopy is perhaps the most valuable because it provides readily distinguishable signatures of each of the different forms of carbon (e.g. diamond, graphite, buckyballs). In addition it is non-destructive, requires little or no specimen preparation, is performed in air and can produce spatially resolved maps of the different forms of carbon within a specimen. This article begins by reviewing the strengths (and some of the pitfalls) of the Raman technique for the analysis of diamond and diamond films and surveys some of the latest developments (for example, surface-enhanced Raman and ultraviolet Raman spectroscopy) which hold the promise of providing a more profound understanding of the outstanding properties of these materials. The remainder of the article is devoted to the uses of Raman spectroscopy in diamond science and technology. Topics covered include using Raman spectroscopy to assess stress, crystalline perfection, phase purity, crystallite size, point defects and doping in diamond and diamond films.

Keywords: Raman spectroscopy; diamond and diamond films; doping; annealing; surface-enhanced Raman scattering (SERS); UV Raman

1. Introduction

(*a*) *Introductory comments*

Laser Raman spectroscopy is widely used as a diagnostic tool for the evaluation of diamond and chemical vapour deposited (CVD) diamond films. The technique is popular because each carbon allotrope displays a clearly identifiable Raman signature, it is non-destructive, requires little or no specimen preparation and can be made confocal so that volumes as small as $1 \times 1 \times 2\,\mu m^3$ can be sampled. Raman scattering from single-crystal and CVD diamond films has recently been reviewed by Zaitsev (2001), who, in addition to describing the fundamental properties of the Raman spectra of single-crystal and CVD films, provides a comprehensive list of nearly all the Raman lines that have been reported in the literature. The present

One contribution of 13 to a Theme 'Raman spectroscopy in carbons: from nanotubes to diamond'.

review, necessarily selective, concentrates on those aspects which the authors feel will be of most use to researchers interested in using Raman microscopy for the evaluation of properties of the diamond materials synthesized or modified in the laboratory. We begin with a very brief review of the Raman spectrum of single-crystal diamond and CVD diamond films. We restrict our attention to single-crystal diamond and to polycrystalline films with relatively large grain sizes. The extensive literature on nanocrystalline diamond and amorphous carbon is reviewed elsewhere in this issue. We describe the potential of two relatively underused techniques for the Raman analysis of diamond, namely, ultraviolet (UV) and surface-enhanced Raman spectroscopy. The increased availability of UV lasers and spectrometers offers an excellent opportunity to gain new insights into CVD diamond growth. We suggest that a full characterization of diamond films will benefit enormously from the use of multiple excitation wavelengths (§ 1 *c*). Surface-enhanced Raman (§ 1 *d*) has the potential to reveal details of the surface bonding, and may one day soon be incorporated into near-field probes capable of providing Raman spatial resolution of the order of 100 nm.

Having surveyed the latest developments in Raman techniques, we devote the rest of the section to reviewing some of the uses of Raman in diamond science and technology. We begin with the most ubiquitous application, namely, the use of Raman in the evaluation of CVD diamond films, and in so doing sound a warning of some of the pitfalls which await those attempting to use Raman for the evaluation of the phase 'purity' and perfection in CVD diamond. Section 2 *b* reviews the use of the Raman shift to estimate the inherent stress in diamond and diamond films, and in § 2 *c* we provide a critical assessment of the phonon confinement model for the evaluation of the crystallite size. An interesting application of Raman is its use as a non-contact thermometer during diamond growth and processing, and this is reviewed in § 2 *d*. In § 2 *e*, we show that Raman provides an extremely convenient method for monitoring point defects in diamond and can be used to provide a semi-quantitative measure of defect annealing. Finally, in § 2 *f*, we describe partially successful attempts to employ Raman to investigate doping of diamond and diamond films.

(*b*) *Raman of the single-crystal and CVD diamond films*

The Raman spectrum of single-crystal diamond (see figure 1) is dominated by the first-order Raman line at 1332 cm^{-1} (full-width half-maximum (FWHM) 1.2 cm^{-1}), which corresponds to the vibrations of the two interpenetrating cubic sublattices. For an infinite lattice only the zone-centre phonon modes are observed in the first-order spectrum, a requirement which is relaxed when the crystallite size is reduced (see § 2 *c*). Hexagonal diamond (i.e. lonsdalite) displays a peak at 1325 cm^{-1} (Bhargava *et al*. 1995; Knight & White 1989). If $^{13}\mathrm{C}$ is substituted for $^{12}\mathrm{C}$ ($^{12}\mathrm{C}_{1-x}{}^{13}\mathrm{C}_x$), the first-order peak for cubic diamond moves down in energy, according to the relationship ω (in cm^{-1}) $= 1332.82 - 34.77x - 16.98x^2$. The first-order diamond mode has been extensively studied, and its behaviour as a function of temperature and applied stress is by now well known (see Zaitsev (2001) and references therein).

The first-order Raman modes are triply degenerate TO(X) phonons of $\mathrm{F}_{2\mathrm{g}}$ symmetry. In an isotropic diamond crystal they consist of one longitudinal mode (singlet) relative to the direction of propagation and two degenerate transverse (doublet) modes. The Raman selection rules for diamond can be derived based on the analysis first introduced by Louden (1964). Table 1 (Stuart 1993; Gardiner & Graves

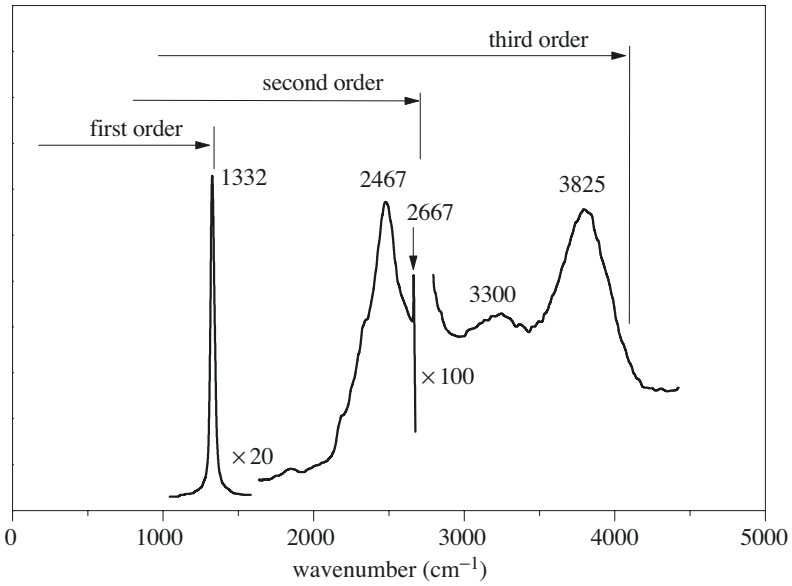

Figure 1. General Raman spectrum of gem-quality diamond excited at room temperature at a wavelength of 228.9 nm. The first-, second- and third-order Raman peaks are shown. (From original data by Bormett *et al.* (1995), as redrawn by Zaitsev (2001).)

Table 1. *Raman scattering intensities for backscattering geometry from* (100) *and* (111) *diamond surfaces (after Stuart 1993)*

(L refers to the longitudinal mode, T_1 and T_2 to the transverse modes. d is a matrix element in the polarizability tensor. For z parallel to [001], θ is defined as the angle between the polarization vector of the incoming laser beam and the [100] direction of the crystal. For z parallel to [111], θ is defined as the angle between the polarization vector of the incoming laser beam and the $[\bar{1}10]$ direction.)

crystal face	mode	$I_\perp$	$I_\parallel$	$I_\perp/I_\parallel$
(001)	L	$d^2\cos^2 2\theta$	$d^2\sin^2 2\theta$	—
	T_1	0	0	—
	T_2	0	0	—
	total	$d^2\cos^2 2\theta$	$d^2\sin^2 2\theta$	$\cos^2 2\theta/\sin^2 2\theta$
(111)	L	0	$d^2/3$	—
	T_1	$(2d^2/3)\sin^2 2\theta$	$(2d^2/3)\cos^2 2\theta$	—
	T_2	$(2d^2/3)\cos^2 2\theta$	$(2d^2/3)\sin^2 2\theta$	—
	total	$2d^2/3$	d^2	2/3

1989) provides a summary of the expected scattering intensities for diamond for the backscattering geometry commonly employed in confocal Raman microscopes. In table 1, the laser is assumed to be incident along the z-axis, where z is parallel to either the [001] or [111] crystallographic direction in the diamond crystal. For z parallel to [001], the incident polarization of the input laser beam is in the (x, y)-plane and θ is defined as the angle between the incident polarization vector

Table 2. *Assignments for Raman peaks commonly observed in CVD diamond films*

position (cm^{-1})	typical FWHM (cm^{-1})	assignment
520	3–5	first-order silicon Raman peak
1100–1150	40–80	most likely transpolyacetylene at grain boundaries (Ferrari & Robertson 2001); Often observed in nanocrystalline CVD diamond films.
1332	5–10	first-order diamond Raman line
1345	250	sp^2 amorphous carbon (the D peak)
1430–1470	80	most likely transpolyacetylene at grain boundaries (Ferrari & Robertson 2001)
1520–1580	100	sp^2 amorphous carbon (the G peak)

and the [100] direction. An analyser can be used to select the direction of polarization of the scattering light. We define two scattering intensities, namely, $I_{\|}$ and $I_{\perp}$, corresponding to the polarization vector of the scattered light being parallel or perpendicular to the polarization direction of the incident laser, respectively. The table shows that scattering from the (100) diamond surface is strongly polarized and moreover strongly dependent on the relative azimuthal orientation of the input polarization with respect to the [100] direction in the crystal. For z parallel to [111], θ is defined as the angle between the input polarization vector and the $[\bar{1}10]$ direction. In this case, the scattering intensity is independent of the azimuthal polarization of the incident light. These selection rules are especially important when using micro Raman spectroscopy to assess the quality and perfection of CVD diamond (see § 2 *a*).

The Raman spectrum of a typical unintentionally doped CVD diamond film is shown in figure 2. In addition to the first-order Raman line at $1332\,cm^{-1}$, peaks appear which for the most part reflect sp^2 bonded components of the films, either in the bulk or in grain boundaries. Typical peak positions and assignments are shown in table 2.

The peaks are often fitted with a combination of Gaussians and Lorentzians with a sloping background. This background is usually due to photoluminescence (PL), often attributable to the neutral nitrogen-vacancy complex $[N\text{-}V]^0$ (575 nm) or the charged nitrogen-vacancy complex $[N\text{-}V]^-$ (638 nm) optical centres, but can also be due to Si (738 nm), or W (717 nm) (Harris *et al*. 1996) incorporation into the films. It can be very useful to extend the spectral scan to include the region where these peaks occur. In this case the Raman line can be used to normalize the spectra in order to obtain a semi-quantitative measure of the incorporation of such impurities into the diamond lattice as a function of growth conditions. A discussion of the myriad PL active peaks in diamond is beyond the scope of this section; a full compendium can be found in Zaitsev (2001, § 5).

(*c*) *Wavelength dependent effects: UV excitation*

Wagner *et al*. (1991) were the first to show the dramatic effects of changing the excitation wavelength on the Raman spectra of CVD diamond films. For example,

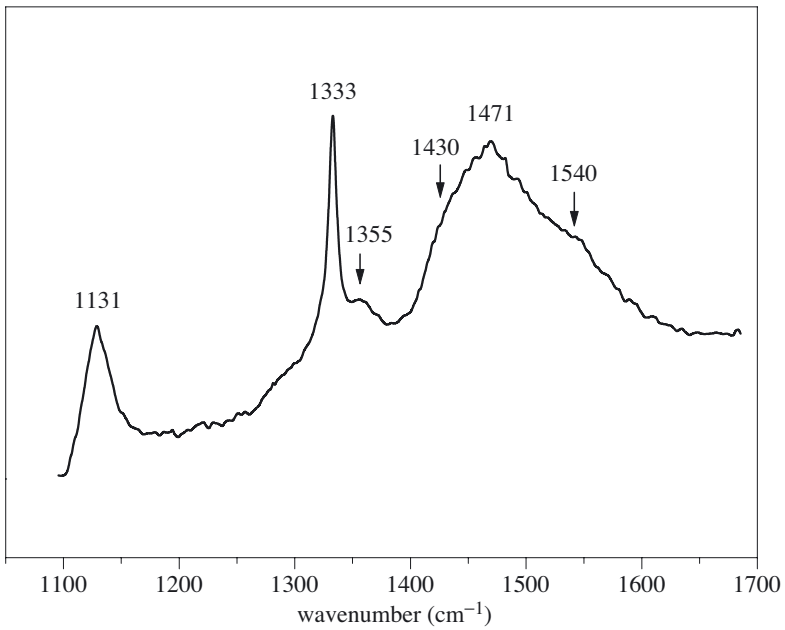

Figure 2. Typical spectrum of CVD diamond film deposited on Mo substrate, at 820 °C. (After Loh & Cappelli (1993), as redrawn by Zaitsev (2001).)

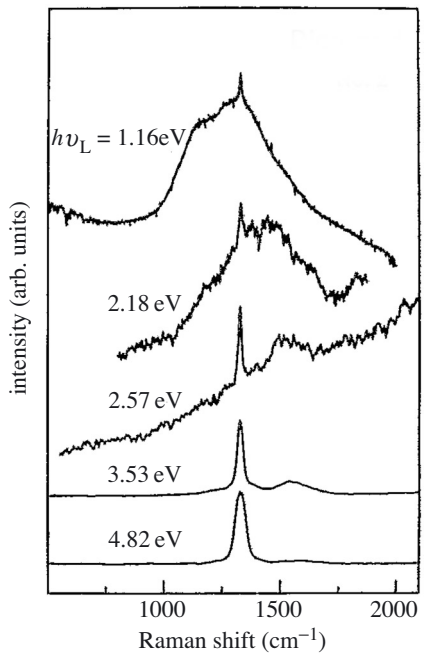

Figure 3. Raman spectrum of a polycrystalline diamond film as a function of excitation wavelength. (After Wagner *et al.* (1991).)

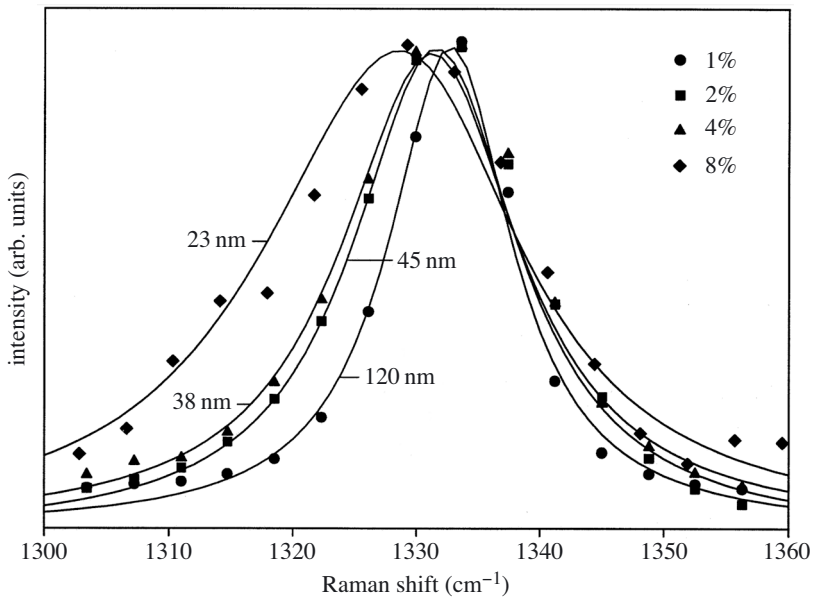

Figure 4. UV Raman spectra for the diamond peak depending on the grain size. Solid line denotes data from the phonon confinement model, symbols those from the experiment. The percentages in the legend refer to the CH_4/H_2 ratio in the gas mix used to produce the diamond films. (After Sun *et al.* (2000).)

figure 3 shows the result for a moderate quality CVD film synthesized by microwave plasma CVD as the excitation wavelength is varied from 257 to 1064 nm. Clearly, the resonant enhancement of the sp^2 and sp^3 bonded portions of the films is very strongly dependent on the excitation wavelength, with the ratio I(diamond)/I(non-diamond) increasing dramatically as the excitation wavelength decreases into the UV. The trends for nanocrystalline films can be even more dramatic in that the first-order diamond peak is only visible for UV excitation. Based on these data alone, it was not possible to determine if the results observed were due to resonant enhancement of the diamond peak, a decrease in resonance of the sp^2 bonded portion of the film or, in fact, some other mechanism, such as preferential absorption of the sp^2 components of the film. However, from a practical point of view, it is clear that the sensitivity to the diamond component is maximized by using UV excitation, whereas the sensitivity to the non-diamond inclusions is maximized by using near-infra-red excitation. This trend in this early work has been confirmed by later studies (see, for example, Leeds *et al.* 1998). The use of UV excitation to study boron-doped films (Wang *et al.* 2002) is discussed further in § 2 *f*.

Sun *et al.* (2000) used the enhanced sensitivity of the first-order Raman line in the UV (244 nm) to show the effect of decreasing crystallite size in nanocrystalline films using the phonon confinement model. Figure 4 shows the line shape of the first-order line as a function of the CH_4/H_2 ratio. As this ratio increases, the crystallite size decreases and the Raman peak moves down in energy and skews. The solid lines are fits to the phonon confinement model for the crystallite size shown in the diagram. For comparison, the crystallite sizes estimated using X-ray photoelectron spectroscopy (XPS) were 120, 40, 34 and 28 nm for samples produced with CH_4/H_2

ratios of 1, 2, 4 and 8%, respectively. Such an analysis was impossible using 514.5 nm excitation because the non-diamond peaks swamped the first-order diamond line.

It should also be noted that the UV spectrum is free of interference from the PL background that is often present when 514 nm excitation is used. This enables spectra to be collected at much a higher signal-to-noise ratio. One interesting application of this is the *in situ* monitoring of the first-order diamond peak in a microwave-plasma CVD reactor. The emission from the microwave plasma (whose intensity falls off sharply below 260 nm) is easily subtracted off. Asher & Bormett (2000) estimate that the system is capable of a 1 nm detection limit for the growing film. The position of the peak can also be used to determine the temperature of the growing film (see § 2 *d*).

Bormett *et al*. (1995) have provided one of the most detailed studies of UV Raman spectroscopy of diamond and carbon allotropes. The absence of the fluorescence background allowed them to observe in detail the first-, second- and third-order phonon bands from diamond (see figure 1), highly oriented pyrolytic graphite (HOPG), glassy carbon and microcrystalline graphite as a prelude to the study of CVD diamond films. A summary of the trends observed when using UV excitation is as follows.

(i) I(diamond)/I(non-diamond) for 244 nm excitation is enhanced by a factor of at least 25 compared with measurements taken using 488 nm excitation. According to Bormett *et al*. (1995), this is primarily due to a decrease in the Raman scattering cross-section for the non-diamond component rather than a resonance enhancement of the first-order Raman line.

(ii) The frequency of the non-diamond band at 1550 cm^{-1} shows a slight increase with increase in excitation frequency.

(iii) The 'D' band at 1355 cm^{-1} and its overtones at combination bands at 2450, 2725 and 2950 cm^{-1} disappear for 244 or 228.9 nm excitation.

The disappearance of the D peak and its overtones for UV excitation of pure graphitically bonded materials and the near-complete absence of background fluorescence are fortunate because it is in this spectral region that one might expect to find evidence of C–H bonding in CVD diamond films. Indeed, the ratio of a peak at 2930 cm^{-1} to that of the first-order phonon line was used to estimate the amount of hydrogen in the films based on the C–H Raman stretching band. A detection limit of 0.001% is apparently possible (Bormett *et al*. 1995).

In summary, it is now clear that a full characterization of CVD diamond films can benefit enormously from the use of multiple wavelength excitation. In particular, the elimination of PL background when using 244 or 229 nm excitation appears to increase the information available from Raman spectroscopy to include detailed measurements of the line shape and width of the first-order phonon even for nanocrystalline CVD films and the ability to estimate the hydrogen content of the films using the second-order spectra. With these capabilities, UV Raman may well compete with near-edge X-ray absorption fine structure (NEXAFS) for the characterization of nanocrystalline diamond materials (Zuiker *et al*. 1996), especially since the former offers micrometre-scale spatial resolution.

A number of developments in instrumentation are noteworthy. The first is the availability of intra-cavity-doubled, continuous-wave Argon ion lasers, which provide

a ready source of 244 nm excitation. Such continuous-wave sources are superior to the previously used pulsed sources because they reduce the possibility of nonlinear effects and laser damage (both to the sample and to the spectrometer optics!). The second is the availability of high-throughput Raman spectrometers coupled to high-power microscopes, which take advantage of high-performance dielectric edge filters allowing the Raman spectrum to be collected down to as low as 400 cm^{-1}. One of the latest developments has been the successful integration of near-field scanning optical microscopy (NSOM) and Raman spectroscopy for UV excitation (Sands *et al*. 2002). Although still in its infancy, this technique has the promise to improve the lateral resolution down to 100 nm, perhaps allowing the investigation of the grain boundaries in nanocrystalline diamond materials. Still lacking, however, is a full resonant Raman investigation using variable wavelengths that span across the indirect (225 nm) and perhaps even the direct band gap (170 nm) of diamond.

(*d*) *Surface enhanced Raman spectroscopy (SERS) of diamond and diamond films*

The skin depth of visible light in diamond is of the order of hundreds of nanometres; hence normal Raman microscopy is not sensitive to the surface structure of diamond films, even when performed confocally. However, when a thin layer of metallic particles (usually Ag) is deposited on to a diamond surface, the Raman signal from the near-surface area can be enhanced by, typically, factors of 10^3–10^8. In addition, SERS tends to quench the luminescence through a radiationless transfer to the metal surface (Campion & Kambhanpati 1998). Although the exact mechanism remains somewhat controversial, it is commonly accepted that it is connected to the enhancement of the local electric field due to the surface plasmons of the metallic particles. Hence the degree of enhancement depends on the metal particle size and shape. The optimization of the properties of the metal coating appear at present to be somewhat empirical. Nevertheless, some extremely useful insights have been gained using this technique.

Knight *et al*. (1990) were perhaps the first to apply the surface-enhanced technique to CVD diamond. They used direct-current magnetron sputtering to coat thin (30–120 nm) CVD diamond films with 5 nm thick Ag layers. It is believed that the optimal thickness for SERS should occur when the optical absorption in the metallic coating is a maximum at the excitation wavelength. In this case, tests of Ag thin films deposited on glass showed minima in the transmission at *ca*. 480 nm for 5 nm Ag films. Thicker films resulted in reduced transmission across the whole wavelength range. Hence for the Raman excitation wavelengths employed (514 and 488 nm), 5 nm Ag films were used.

Figure 5 shows the dramatic enhancement following the Ag coating. The CVD diamond film was 20–40 nm in thickness. Without the Ag coating the Raman spectrum fails to reveal any sign of the CVD coating (figure 5*a*). Indeed, the spectrum is indistinguishable from that obtained from a bare silicon substrate. By contrast, with the 5 nm Ag films, the Raman spectrum reveals the signature of a typical CVD film superimposed with signals from amorphous carbon (figure 5*b*). When Ag was deposited on a bare silicon substrate, peaks at 1340 and 1604 cm^{-1} were also observed, but no peak at 1332 cm^{-1} could be seen. Hence, it is possible that some of the non-diamond features in figure 5 may have contributions from adventitious surface carbon or carbon incorporated into the Ag coating. Nevertheless, this work

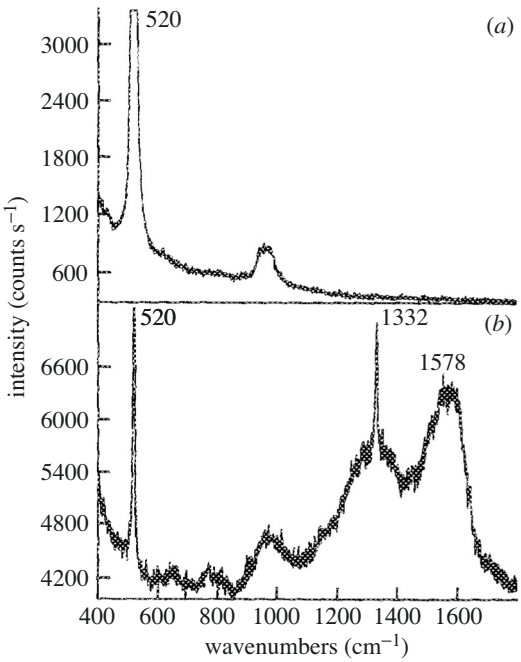

Figure 5. Raman spectra of a thin (20–40 nm) CVD diamond film deposited on silicon. (*a*) Raman spectrum without an Ag coating. (*b*) The same film with the silver overlayer. (After Knight *et al*. (1990).)

showed that SERS could provide a pronounced enhancement of the surface sensitivity of the Raman technique for diamond. The results showed that the formation of diamond occurs at a very early stage in the CVD process. In retrospect, this work indicated that, provided that a sufficiently high nucleation density can be achieved by appropriate seeding, ultrathin continuous CVD diamond layers could be realized.

Later work concentrated on the evaluation of the surface structure of CVD diamond, with rather surprising results. Okada *et al*. (1992) used SERS to investigate CVD diamond synthesized by the combustion flame method. In this case the films were thick, with grain sizes of 5–10 μm. Normal Raman microscopy showed only the first-order Raman peak at 1332 cm^{-1}. The SERS spectrum showed strong peaks at 1580 and 1355 cm^{-1} with only a small first-order diamond peak at 1332 cm^{-1}. The authors concluded that the surface of CVD diamond has a sp^2-like structure, possibly due to the 2×1 dimer formation and the absorption of C_2H_2 and/or acetylenic species on the surface. Huang *et al*. (2000) experimented with different metals and concluded that metals with smaller work functions (e.g. In) could give even higher surface enhancement than Au and Ag. It is interesting to note that some researchers (Fleishman *et al*. 1974) claim that charge transfer between adsorbates and the metal surface can result in a change of polarizability, yielding strong SERS selectivity for surface species.

Elegant experiments were performed by López-Ríos *et al*. (1996). The improved methodology involved performing the SERS experiments *in situ* in the CVD deposition chamber. After a CVD diamond film was deposited on to a scratched silicon substrate, Ag films were deposited on to the diamond film while the SERS out-

put was monitored and the deposition was stopped when the SERS signal was at its maximum. The most dramatic effects were observed when the CVD film was heated to 850 °C before the Ag deposition. In that case, strong peaks at 1127 and 1427 cm^{-1} were observed, which were attributed to the formation of trans-$(CH)_n$ (i.e. polyacetylene). In addition, a pronounced asymmetry in the first-order diamond peak was observed. As will be discussed below (see § 2 *c*), this asymmetry is usually interpreted in terms of phonon confinement in nanometre sized diamond particles. A very small peak was also observed at *ca.* 1240 cm^{-1} (López-Ríos 1996), which was attributed to the peak in the phonon density of states (PDOS) of diamond which would also be expected to be observed for very small particles.

SERS can also be used to study the interaction of adsorbates on single-crystal diamond surfaces. Ushizawa *et al.* (1999) used SERS to study hydrogenated and deuterated (100) and (111) diamond surfaces. Multiple peaks in the vicinity of 2700–3100 and 2000–2300 cm^{-1} were observed for hydrogenated and deuterated species, respectively. They compared their results with those obtained using high-resolution electron energy loss spectroscopy (HREELS) and Fourier transform infrared (FT-IR) and found in general good agreement between the different surface techniques and with *ab initio* molecular orbital calculations, which all showed that the (100) surface was terminated with C–H monohydride species. SERS has certain advantages over HREELS for this application, namely that the spectral resolution is higher allowing single peaks observed in HREELS to be resolved into individual components, and that the spatial resolution of SERS is of the order of 1 μm, allowing very small samples to be used. For example, it is possible to compare the SERS spectrum from the (100) and (111) oriented facets of a CVD film, which is usually not possible using HREELS since these techniques require large crystals, a few millimetres in diameter.

Table 3 summarizes the peak assignment from SERS results taken from a number of authors (after Roy *et al.* 2002*a*). The appearance of features in the SERS spectrum which can be identified in the PDOS of diamond or graphite are consistent with the observation of nanoscale structures on the diamond surface. Note that there is still considerable uncertainty in the interpretation of the SERS results. For example, it is not known if the SERS spectrum originates from within the diamond grains or from grain boundaries.

Despite very convincing arguments by Ferrari & Robertson (2001), the identification of the peaks at 1460 cm^{-1} and 1170 cm^{-1} as due to trans-polyacetylene is still controversial. The former is often quite broad, and this would seem to be incompatible with assignment to such a specific molecular species. Comparing with silicon, the latter mode could correspond to the 650 cm^{-1} branch that is often observed in Raman from a-Si (which has been assigned to an Si–H bending mode). It is also possible that this mode has more than one component. It is sometimes sharp (which one might argue is due to hydrogen) and it is sometimes broad and step shaped (more like a density-of-states feature). In some nanocrystalline films, the substitution of deuterium for hydrogen in the growth mixture causes the peak to disappear, which would support the idea of it being connected with hydrogen (Pfeiffer *et al.* 2003).

In summary, SERS has been found to be an extremely useful technique for the analysis of the near-surface structure of diamond and diamond films. When applied to single-crystal diamond surfaces, it can be used to probe chemisorption as a viable alternative to HREELS, especially if only very small samples are available or if it is desired to probe differences in chemisorption on different facets of crystals grown in

Table 3. *Assignment of peaks observed in SERS spectra (after Roy et al. (2002a))*

peak position (cm^{-1})	possible origin	comments	references
1600	G peak of amorphous carbon	matches with maximum in the PDOS of graphite	Knight & White (1989)
1460	trans-polyacetylene	observed as a strong peak when CVD diamond is annealed at 850 °C; assignment is still controversial	López-Ríos *et al.* (1996); Ferrari & Robertson (2001)
1350	D peak from amorphous carbon		Knight & White (1989)
1333	first-order Raman	peak grows in intensity with increasing SERS effect, but suffers a red shift and is skewed to lower wavenumbers, consistent with the breakdown of the selection rules in nm-sized diamond crystals	Roy *et al.* (2002*b*)
1240–1280	corresponds to a maximum in the PDOS of diamond, but may also be due to trans-poly-acetylene, which has a small Raman peak at 1240 cm^{-1}	appearance of such a structure is concomitant with the above changes in the first-order Raman line	López-Ríos (1996); Roy *et al.* (2002*a*, *b*); Ferrari & Robertson (2001)
1170	trans-polacetylene	observed as a strong peak when CVD diamond is annealed at 850 °C; assignment is still somewhat controversial, although Ferrari & Robertson (2001) provide much convincing evidence for trans-polyacetylene assignment	López-Ríos (1996); Ferrari & Robertson (2001)

the CVD environment. Interestingly, SERS has revealed the existence of nanophases at the surface which are not present in the bulk. Future developments of this technique may involve the combination of surface enhancement with NSOM to provide lateral spatial distribution of the order of 100 nm or less. Such a combination may be accomplished by coating the end of NSOM tips with appropriate Ag coatings. Combined with the nanometre depth sensitivity of SERS, NSOM could offer new insights into the grain structure of diamond and nanostructured diamond films.

2. Applications of Raman spectroscopy in diamond science

(*a*) *Measuring the phase purity and crystalline perfection of CVD diamond*

Given that the Raman spectrum of CVD diamond can be deconvolved into peaks that can be attributed to diamond and non-diamond components of the film (see § 1 *b*), it is not surprising that many authors (see, for example, Prawer *et al*. 1991; Harris *et al*. 1996) have used the ratio $I(1332)/I(1500)$ as a measure of the phase purity of diamond films. For example, the observation of a 1332 cm^{-1} line on a flat background with no observable peak in the region 1500–1550 cm^{-1} is often taken as strong evidence for the production of 'pure' diamond with virtually no non-diamond components present. This is particularly the case if the measurement is carried out using infrared (IR) excitation, which enhances the Raman sensitivity to the sp^2 component of the film. Furthermore, the FWHM of the Raman line is often taken as a measure of the 'perfection' of the diamond crystallite, with the peak position being used as an estimate of the residual stress.

While these measures can be extremely useful in mapping the deposition parameter space, they must be used with caution. A number of often overlooked factors can influence these ratios in quite a dramatic fashion, particularly when micro, rather than macro Raman measurements are employed. For example, Prawer *et al*. (1994) showed that the crystallite orientation with respect to the E vector of the incoming laser irradiation can dramatically effect the ratio $I(1332)/I(1500)$. This is because the Raman scattering from the non-diamond components is almost completely depolarized, whereas the scattering from the crystalline diamond component shows a strong polarization dependence (see § 1 *b*). Thus, just rotating a crystallite under the laser beam yields a different estimate of the diamond quality (sometimes by up to a factor of 10). Thus, the observed differences in the micro Raman spectra of adjacent crystallites may in some cases be due to the orientational dependence of the Raman spectra, rather than any intrinsic spatial inhomogeneity. The position, width and shape of the first-order diamond line also shows a strong polarization dependence (Stuart *et al*. 1993*a*, *b*; Harris *et al*. 1996), which, if ignored, can lead to misleading conclusions regarding residual stress in the films. In particular, changing the polarization can change the measured FWHM of the first-order line; therefore caution should be exercised in employing the FWHM as a measure of crystalline 'quality'.

Another factor often overlooked is the very large inhomogeneity that can occur within a single crystallite. Confocal Raman measurements (Stuart *et al*. 1993*b*; Nugent & Prawer 1998) reveal large variations between different points on the crystal separated by as little as 1 μm. Peak splitting was often observed, with the first-order peak consisting of two and sometimes three components. Stress-induced splitting into a singlet and doublet (see § 2 *b*) has sometimes been invoked to explain such data; however, we consider it more likely that the observed splitting derives from

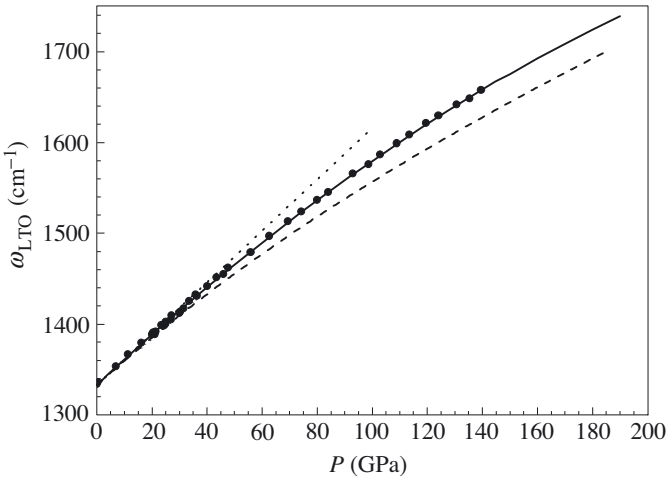

Figure 6. The observed Raman frequency of the F_{2g} mode versus pressure. The dotted line represents the slope at zero pressure (i.e. a_1 in equation (2.1)), the solid line represents the fit to the data using equation (2.1), and the dashed line represents the results of calculations. (Reproduced with permission from Occelli *et al.* (2003).)

the fact that the confocal Raman probe samples more than one growth sector in the CVD film. The presence of high concentrations of defects in the (111) growth sectors results in an overall tensile strain in these regions. By contrast the (100) growth sectors appear to be under compressive stress. This sector-like growth (see, for example, Tarutani *et al.* 1995) can result in inhomogeneous broadening of the Raman line which can be mistaken for an increase in the defect level within the material. Such inhomogeneous broadening can also explain why macro Raman measurements often return an FWHM which is much larger than that obtained from micro Raman measurements.

(*b*) *Stress and pressure dependence*

Under hydrostatic pressure the triply degenerate F_{2g} first-order Raman peak remains degenerate and is shifted to higher frequency (see figure 6). There have been several careful studies of the Raman peak frequency versus pressure with the recent study of Occelli *et al.* (2003) reporting values up to 140 GPa. At this pressure, the first-order mode was observed to shift to above 1650 cm^{-1} while maintaining a linewidth increase of only 2 cm^{-1}. The data were fitted to a quadratic expression

$$\omega(P) = \omega_0 + a_1 P + a_2 P^2, \tag{2.1}$$

where $\omega_0 = 1333.0$, $a_1 = 2.83\,\mathrm{cm}^{-1}\,\mathrm{GPa}^{-1}$ and $a_2 = -3.65 \times 10^{-3}\,\mathrm{cm}^{-1}\,\mathrm{GPa}^{-2}$. The value of a_1 is in essential agreement with several prior studies where the measurements were confined to pressures less than 40 GPa.

The analysis indicated that the ratio of the bond-stretching and bond-bending force constants varied with pressure. The results suggested that the covalent bonding strength increased with pressure, which is not typical of most materials.

Kunc *et al.* (2003) argued with several aspects of this analysis. They noted that the use of equation (2.1) may be inappropriate because pressure is not an independent variable. They also noted that most theoretical studies to date indicated a

disagreement with the experimental results. This difference may be explained by a variation in the pressure calibration of the measurements. In fact, there has been previous discussion that the pressure calibration based on ruby fluorescence may need to be corrected. The disagreements become significant for values above 40 GPa. If this difference in the experimental results and the theoretical predictions is substantiated, it could be argued that the bonding in diamond is strengthened at increased pressures (Occelli *et al*. 2003). It is evident that more careful measurements at even higher pressures could be significant for understanding the nature of the bonding in diamond.

Under uniaxial stress, the degeneracy of the F_{2g} first-order mode is lifted and mode splitting has been predicted and observed. Grimsditch *et al*. (1978) measured the frequency and splitting of the first-order Raman peak for uniaxial stress along [001] and [111] directions. A stress of up to 1 GPa was applied to crystals cut with long axis along the [001] and [111] directions. In both cases the triply degenerate mode splits into a singlet and doublet. It was shown that different polarization configurations could be used to separate the different components, which overlapped in the spectra. The measurements indicated that the mode splitting followed the relations

$$\Delta\omega_{[111]} = 2.2 \pm 0.2\ \mathrm{cm}^{-1}\ \mathrm{GPa}^{-1},$$

$$\Delta\omega_{[001]} = 0.73 \pm 0.10\ \mathrm{cm}^{-1}\ \mathrm{GPa}^{-1},$$

and the hydrostatic component followed the relation

$$\Delta\omega_{\mathrm{H}} = 3.2 \pm 0.23\ \mathrm{cm}^{-1}\ \mathrm{GPa}^{-1}.$$

They also deduced the mode Gruneisen parameter and the third-order elastic constants. These values of the bulk properties can then be employed to analyse the stress in thin films.

With the results on single crystals as a basis, Raman scattering has been applied to analyse the stress state of diamond films. Residual stress after film growth can be due to the difference in the thermal expansion of the film and the substrate, and other effects including lattice mismatch, bonding at grain boundaries and bonding changes during film growth. The latter two effects are sometimes termed intrinsic stress. The first effect is typically dominant in the growth of polycrystalline films.

In polycrystalline films, it is assumed that the measurement samples a sufficient number of grains and that the signal represents an average of all grain orientations. The stress, however, may have a particular relation to the substrate or growth surface.

For small stress, the Raman spectra will display a single peak shifted from the natural frequency. The peak may be broadened by stress-induced splitting of the triply degenerate mode and also from non-uniformities in the stress distribution. For these small stresses, a hydrostatic model has often been applied to deduce the stress. In general, there has been disagreement between these measurements and the stress measured from other techniques such as wafer bending. Windischmann & Gray (1995) argued that for stress generated during film growth, the hydostatic model underestimates the actual stress by 50%, since the film growth usually results in biaxial stress. The biaxial stress can be described as a combination of two-thirds hydrostatic and one-third uniaxial stress. This approach is appropriate when the stress state is such that mode splitting is not detectable. Thus when the measurements are corrected for this factor of 1.5, the Raman deduced stress results are in more reasonable agreement with other approaches.

The analysis of stress in polycrystalline films has been carefully considered theoretically by Ager & Drory (1993) and Anastassakis (1999). The study by Ager & Drory determined the stress shifts by assuming a biaxial stress in a random polycrystalline film. The approach involved calculation of the frequencies using the phonon secular equation in four separate directions and then averaging. The model was employed to analyse results of diamond film deposited on a titanium alloy, and the results were consistent with a biaxial residual stress of 7.1 GPa.

Anastassakis (1999) employed a more general approach to analyse the splitting and the relative intensity of the modes for different stress distributions in a polycrystalline film. The analysis assumed that the Raman measurements sampled a large number of randomly oriented domains, and that the stress state in the assembly was the same in each domain. The approach involved determining the phonon deformation potentials of the polycrystalline film. The analysis is applied to different stress states. For uniaxial stress the results indicate two modes, a singlet and doublet, where the intensity of the doublet is twice that of the singlet. The analysis notes that the stress state termed 'bisotropic' is a more correct terminology for the commonly used 'biaxial stress' ascribed to stress that occurs during film growth. The purely bisotropic case again results in a singlet and doublet with the same 1:2 intensity ratio. The calculated mode shifting versus stress finds that the doublet mode shifts to a greater degree than the singlet, with the calculated singlet/doublet ratio of the stress shift to be approximately 0.39. The analysis also notes that polarization cannot be employed to separate the different modes because the angular averaging indicates that both modes will be observed with the same depolarization ratio.

The analysis of Anastassakis (1999) also considered the situation where purely bisotropic stress (or 'biaxial' according to other authors) resulted in an unresolved spectrum. Then the ratio of the biaxial stress and the shift of the unresolved peak was found to be -0.47 (GPa cm^{-1}).

More complicated stress configurations such as biaxial stress (with non-equal components), pure shear stress, or a general stress state, are expected to lead to complete splitting of the triply degenerate mode. The intensity of each component is predicted to be equal, but analysis of the spectra is complicated because the modes will exhibit significant overlap and may not be distinct. These more complex stress distributions are expected to arise for indents and other microstructures. Also, as outlined in the previous section, the inhomogeneity due to the sector-like growth in the CVD diamond films will complicate the analysis.

(*c*) *Phonon confinement effects for finite crystal domains*

For Raman scattering from finite-sized crystals, the wavevector of the vibrational excitation is uncertain by a factor of $\Delta k = 2\pi/L$, where L is the crystal dimension. This result is obtained from either the Heisenberg uncertainty principle or from an analysis of the Fourier transform of a finite spatial wave. Thus the momentum or wavevector selection rules for Raman scattering from a finite-sized crystal will be uncertain to this degree. In essentially simultaneous and independent reports, Richter *et al*. (1981) and Nemanich *et al*. (1981) analysed how this effect would be manifested in the Raman spectra. Both studies considered a similar approach where the Raman scattering from a sample would be construed to measure a large distribution of different domains such that the modes of the domains could be approximated by the

phonon dispersion of the infinite crystal. Thus the Raman spectrum would represent signal from all modes in the Brillouin zone within the phonon uncertainty. This effect becomes significant when crystal domains are less than 100 nm. For instance, the Brillouin zone boundary wavevector is π/a, where a is the lattice constant. Thus for a 0.5 nm lattice constant, the wavevector uncertainty for a 100, 10 and 1 nm crystal domains is 1.0, 10.0 and 100%, respectively, of the Brillouin zone boundary wavevector.

Based on the wavevector or momentum selection rules, Raman scattering measures a mode near the centre of the Brillouin zone, (i.e. $k_{\mathrm{p}} \approx 0$). For relatively large wavevector uncertainty (i.e. for $L < 10$ nm) the models of Richter *et al.* (1981) and Nemanich *et al.* (1981) assume that the Raman spectra will be represented by an appropriately weighted Gaussian distribution of the modes within $2\pi/L$ of the zone centre.

Thus, to accurately determine the variation of the Raman spectrum as the domain size is decreased, it is necessary to consider the phonon dispersion of the F_{2g} optic branch. This triply degenerate mode splits as k increases from the zone centre. These effects have been carefully considered in calculations of the phonon confinement effects in the Raman spectra of Si. Detailed calculations by Fauchet & Campbell (1988) indicate that the Raman spectrum is expected to broaden, and the peak frequency is expected to shift towards lower frequency. The broadening is asymmetric to lower phonon frequencies.

LeGrice *et al.* (1990) noted that the phonon dispersion of the F_{2g} optical mode of diamond was similar to that of silicon along the [110] direction. In this direction the branch is nearly degenerate and can be approximated by a straight line. Based on the fact that the slope of the straight line fit in both Si and diamond is similar, they argued that the results for Si were directly applicable to Raman scattering from nanometre-scale domains in diamond.

More recently, Ager *et al.* (1991) have considered specifically the phonon dispersion of diamond. It is notable that there is an unusual case along the [001] direction where one branch disperses slightly upward (by several cm^{-1}) before a downward dispersion trend at increasing wavevector. However, this branch does not seem to strongly affect the results when averaged over all possible directions. In fact, the results from the calculation of Ager *et al.* (1991) are indeed similar to those for Si and substantiate the argument of LeGrice *et al.* (1990).

A more critical effect is the inclusion of lifetime effects and effects due to a distribution of domain sizes. The distribution of domain sizes can be accommodated in the analysis by a Gaussian broadening of the wavevector uncertainty. The lifetime effects will typically lead to a Lorentzian broadening of the peak. This effect should most properly be incorporated for each allowed wavevector and then summed. This is the approach developed by Nemanich *et al.* (1981), but their analysis was applied to hexagonal boron nitride rather than cubic materials.

Thus we have three effects that must be considered in the analysis. If lifetime broadening is negligible and the domain size distribution is relatively uniform, then the analysis of Ager *et al.* (1991) could be a reasonable representation of the Raman spectra. It seems unlikely that this is the case in most realistic examples. It is then necessary to use a combination of Lorentzian and Gaussian broadened curves to describe the results. If the experimental results exhibit a Lorentzian line shape, then it is likely that the lifetime scattering is the dominant effect. If the peak exhibits

a Gaussian line shape, then it is likely that there is a rather broad distribution of domain sizes.

To date, the phonon confinement effects have not been explicitly detected for diamond. The study of Ager *et al.* (1991) highlighted the complexity in the analysis. They measured the Raman spectra at many points on the surface of a series of CVD diamond films. In all cases, the spectra shifted to higher frequency rather than the lower frequency predicted by the confinement model. They concluded that stress effects were dominant over the confinement effects. Bergman & Nemanich (1995) followed a similar analysis and also concluded that the confinement effects were not the most significant in the observed shifts.

(*d*) *Non-contact measurement of temperature*

It is often extremely useful to be able to measure the temperature of a diamond surface using non-contact methods. Some typical applications are to monitor the temperature *in situ* during CVD diamond growth, accurate measurement of the diamond surface temperature in an ultra-high vacuum (UHV) chamber and to monitor the temperature inside a diamond anvil pressure cell. Optical pyrometry is often employed. However, the accuracy of this technique is dependent on the emissivity of the diamond, which in turn depends on impurities, defects, etc. Contact methods using thermocouples suffer from the difficulty of ensuring intimate thermal contact between the diamond sample and the thermocouple, which is especially problematic in UHV environments.

Raman spectroscopy offers an elegant non-contact solution to the problem of temperature measurement. In principle, one of two techniques can be used. Cui *et al.* (1998) provide an excellent comparison of two approaches. The first employs the ratio of the intensities of the Stokes (I_{S}) and anti-Stokes (I_{AS}) peaks, which is given by

$$\frac{I_{\mathrm{AS}}}{I_{\mathrm{S}}} = \left(\frac{\omega_{\mathrm{l}} + \omega_{\mathrm{p}}}{\omega_{\mathrm{l}} - \omega_{\mathrm{p}}}\right)^4 \gamma \mathrm{e}^{\hbar\omega_{\mathrm{p}}/kT}, \tag{2.2}$$

where ω_{l} and ω_{p} refer to the frequencies of the laser and phonons respectively. γ is a factor which takes into account the differences in the detection efficiencies of photons with different energies and is assumed to be temperature independent, but will have to be determined for each particular spectrometer. When detailed and careful calibration measurements are made, this method is found to provide accurate measurements only for $T_{\mathrm{sample}} < 750$ K. Above this temperature, using equation (2.2) results in an overestimate of the sample temperature by up to 75 K. The accuracy of this technique is clearly very sensitive to measurements of absolute intensity ratios and there are many factors which may influence this ratio indirectly, apart from the actual change in temperature, such as, for example, a change in the resonance enhancement due to temperature-dependent changes in the band gap. Cui *et al.* (1998) therefore conclude that the Stokes/anti-Stokes method is ill suited to the accurate temperature measurement of diamond.

The alternative method is to deduce the temperature from changes in the Raman line position. This is very attractive method because typically this position can be measured using curve fitting to within 0.3 cm^{-1}, which translates to a precision in the temperature measurement of *ca.* $\pm$10 K. These shifts originate from anharmonic effects, which act to change the harmonic frequency at the Brillouin zone centre,

to a damped frequency. Liu *et al.* (2000) provide a brief summary of the different decay channels which have been proposed for the decay of the zone-centre phonon. In the case of the decay of the optic phonon into two acoustic phonons with opposite momenta but originating from the same branch, the temperature dependence of the Raman linewidth simplifies to

$$\Gamma(T) = \Gamma_0\left(1 + \frac{2}{\mathrm{e}^{\hbar\omega_0/2kT} - 1}\right), \tag{2.3}$$

where Γ_0 is the linewidth and ω_0 is the zone-centre phonon energy (both at $T = 0$ K). Since the real and imaginary parts of the self-energy are related by the Kramers–Kronig relationship, it follows that the Raman shift at non-zero temperature should follow the same temperature dependence but with opposite sign, i.e.

$$\Delta\omega(T) = -A\left(\frac{2}{\mathrm{e}^{\hbar\omega_0/2kT} - 1}\right), \tag{2.4}$$

where $\Delta\omega$ is the line shift away from ω_0 at non-zero temperature. Indeed, a linear relationship between increase in linewidth and downward Raman shift has been observed in quite a number of examples and it appears that this relationship holds also when the phonon lifetime is reduced by the deliberate introduction of defects (Jamieson *et al.* 1995; Orwa *et al.* 2000).

Cui *et al.* (1998) use a slightly modified version of the above equation and show that it holds over a wide temperature range from 300 to 2000 K. Using data from a number of authors they provide an empirical expression for the conversion of Raman shift to temperature:

$$T = \frac{Dhc\omega_0}{k\ln\{1 + C/[\omega_0 - \omega(T)]\}}, \tag{2.5}$$

with $\omega_0 = 1333\,\mathrm{cm}^{-1}$, $C = 61.14\,\mathrm{cm}^{-1}$ and $D = 0.787$. Using this expression, the temperature of both a single-crystal diamond in air and a CVD diamond crystal in UHV could be measured to within 20 K over a temperature range of 300–1100 K. Despite this success, caution should be exercised in applying equation (2.5) without first calibrating the particular system under examination. For example, strain may affect not only the value of ω_0 but also the temperature dependence of the Raman shift. In other words, although it is likely that the functional form of $\omega(T)$ will follow equation (2.5) for most types of diamond, the values of D and C should not be viewed as universal; they may turn out to depend on crystalline quality, degree of doping and crystallite size.

We conclude this section with a number of interesting examples of the use of the Raman technique to measure local temperature. Schiferl *et al.* (1997) addressed the problem of measuring the temperature and pressure inside a diamond anvil cell. It has been shown that reliable measurement of pressure and temperature requires a separate sensor from the diamond anvils themselves because the shift of the anvil peak has been found to vary with crystallographic orientation of the anvil, and the nature of the gasket and the sample. ^{12}C based diamond chips placed inside the sample chamber have been used for some time; however, the challenge is to separate out the Raman signal from the sensor chip from that of the anvil. The novel solution proposed by Schiferl *et al.* (1997) is to use an additional CVD diamond chip comprised predominantly of ^{13}C whose first-order Raman peak occurs at 1281 cm^{-1},

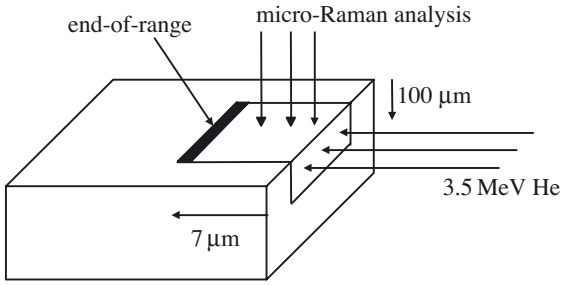

Figure 7. Schematic showing cross-sectional geometry used for the analysis of ion-implantation induced defects in diamond. (After Jamieson *et al.* (1995).) The degree of damage increases with implantation depth reaching a maximum at the end of range.

well separated from the peaks due to the anvils. They report careful calibration of the temperature and pressure dependence of both ^{12}C and ^{13}C diamond, using a different fitting procedure from the one suggested above. Nevertheless, they show that the combination of these two probes is sufficient to be able to measure the pressure (0–25 GPa) and temperature (10–1200 K) of any sample compatible with an externally heated diamond anvil cell.

It is of course well established that the probe laser can cause local heating. This is often not a problem for diamond samples, because of their high thermal conductivity. However, in some instances in which isolated diamond particles are grown on substrates to which they adhere poorly, the effects of laser heating can be dramatic. Laikhtman & Hoffman (1997) grew isolated CVD diamond particles on glassy carbon substrates. They used equation (2.2) to determine the local temperature as a function of laser power and found that the local temperature could reach 1000 K for an input laser power of 15 mW focused into a 2 μm diameter spot. Interestingly, in cases where such large temperature rises were recorded, the diamond particles on the substrate would often disappear, most likely due to local oxidation. Such an extreme case of local temperature rise is rare and indeed samples grown on silicon and continuous CVD films do not usually show such large rises in local temperature. Nevertheless, it is as well to remember that a temperature rise of only 50 K results in a peak shift of *ca.* 1.2 cm^{-1} and that this could easily be erroneously interpreted as being due to strain. Therefore, care must be taken to minimize laser heating effects. A sensible test is to always determine if the peak positions show any dependence on laser input power.

(*e*) *Probing defects and annealing*

While the literature on defect-induced photoluminescence lines in diamond is very rich indeed (see Zaitsev 2001, § 5), there are comparatively few studies reporting Raman active local modes associated with point defects in diamond. One of the most complete studies is that reported by Orwa *et al.* (2000). In this case the point defects were introduced into the diamond by high-energy He-ion irradiation. The somewhat unusual cross-sectional experimental configuration is shown in figure 7. The advantage of this geometry is that the whole of the region sampled by the Raman probe has a uniform level of damage. For these implantations, the damage increases as a function of depth reaching a maximum at the end of range. Figure 8

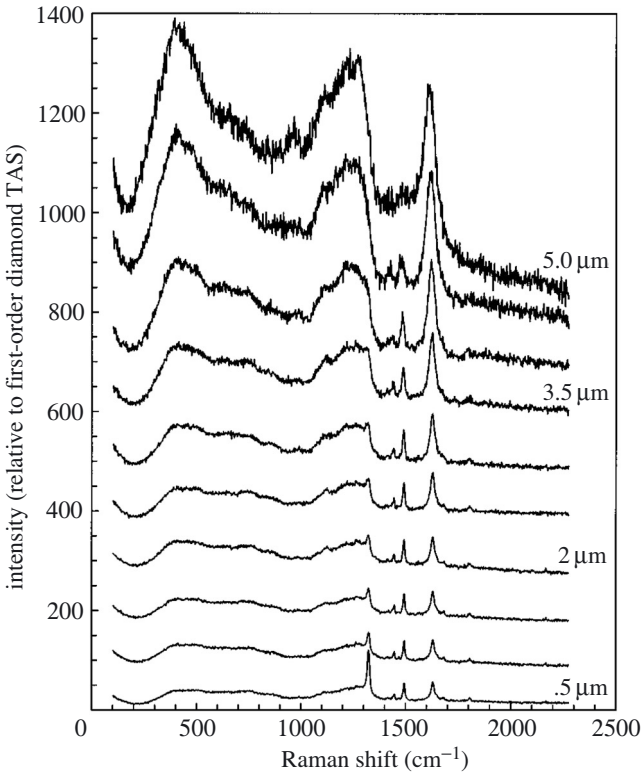

Figure 8. Raman spectra as a function of implantation depth (see figure 7). The degree of damage increases with increasing depth reaching a maximum at the end of range (5 μm).

shows Raman spectra normalized to the first-order Raman line as a function of depth below the surface (i.e. as a function of increasing ion beam damage). These spectra were taken using polarizations of the incoming and outgoing beams such that the first-order Raman line is in fact forbidden and its presence in the spectra is due to polarization leakage in the experimental arrangement (*ca.* 6.5%). The introduction of the defects into the diamond has the following effects on the Raman spectra.

(i) New peaks appear in the Raman spectra at 1490 and 1630 cm^{-1} (185 and 202 meV, respectively). Recent molecular dynamics simulations (Prawer *et al.* 2004) have resulted in the unambiguous identification of these peaks as being due to the vacancy and split interstitial defects, respectively.

(ii) At higher levels of damage, broad structures appear below 1400 cm^{-1} with peaks at *ca.* 500 and 1200 cm^{-1}, which are broadly consistent with peaks in the phonon density of states (PDOS) of diamond. The emergence of such structures is expected because the ion beam creates amorphous zones in which the selection rules break down and allow the observation of features in the PDOS (Prawer *et al.* 1998).

(iii) The first-order peak moves down in energy and broadens. There is a close linear relationship between the downward shift in the Raman peak position and the FWHM of the Raman mode (Jamieson *et al.* 1995; Orwa *et al.* 2000).

These trends are useful and important for a number of reasons. The identification of the 1490 and 1630 cm^{-1} peaks as due to the vacancy and split-interstitial, respectively, means that Raman spectroscopy can be used to study the kinetics of the annealing of point defects in diamond. The presence of such peaks in the Raman spectrum can be used as evidence of residual defects in diamond doped by ion implantation and can therefore be used to help distinguish between electrical conductivity due to residual damage and that due to true chemical doping (Kalish *et al.* 2003). The identification of features in the spectrum due to an amorphous component can also be used to study the recovery of the diamond lattice following implantation damage. The spectra also serve as an important reference for the interpretation of Raman spectra from nanocrystalline diamond (Prawer *et al.* 2000).

One important point to note is the very large downward shift in the first-order Raman peak position with increasing damage (up to 50 cm^{-1}) and the associated broadening of the peak (up to 80 cm^{-1}) (Jamieson *et al.* 1995; Orwa *et al.* 2000). Remarkably, the peak broadening is not accompanied by any skewing or distortion; a single Lorentzian can still be used to fit the broadened peak and a linear relationship between peak shift and FWHM broadening holds over a very wide range. In fact the peak position and FWHM are intrinsically connected by the Kramers–Kronig relationship and are therefore not independent variables. This implies that an increase in defect density in a CVD film can result in a downward shift of the first-order Raman peak position, even if there is no residual stress.

(*f*) *Doping*

Given the importance of the doping of diamond, it is not surprising that many researchers have searched for Raman signatures that could be used to provide a non-destructive, contactless method to assess the level of doping. Unfortunately, there does not appear to be any simple signature, such as, for example, a local Raman active vibrational mode corresponding to a B–C stretch, which can be used for this purpose. Rather, the signatures are more subtle, involving interactions between the vibrational modes of the lattice and the electronic continuum of states induced by the dopants.

In surveying the literature, one needs to differentiate between the following concepts as they relate to doping. The first is the ratio of the dopant to the carbon concentration in the gas mixture. Most authors quote this ratio as $R = [\mathrm{dopant}]/[\mathrm{carbon}]$ in units of ppm, but some authors may use the ppm level of doping in the overall gas mixture, which in general for CVD would be about two orders of magnitude lower. The second is the concentration of dopant (N_{dopant}) in the films. This is not a linear function of R, and in fact depends on many factors, one of the most important of which is the growth direction. For example, in the case of boron doping, for a given value of R, the incorporation of boron is much higher for {111} faces than for {100} faces (Ushizawa *et al.* 1998). Furthermore, there are at least two ways of determining the dopant concentration. The first is secondary-ion mass spectrometry (SIMS), which provides in principle a global measure of the dopant concentration. The second is the use of IR absorption. For boron doping, an IR-active local mode exists which is commonly used to measure the boron concentration in the diamond lattice. Thus the latter measures only those B atoms which are actually incorporated in the lattice; the former measures total incorporated boron including any boron in grain boundaries.

Since the activation energy of most dopants in diamond is large (of the order of 0.3 eV or higher) at room temperature, only about 10^{-3} of dopants will be activated. Thus, unlike the case of Si and Ge, the dopant concentration, N_{dopant}, is expected to be much larger than the electron or hole carrier concentrations (n and p, respectively) and will be a sensitive function of temperature. n and p are generally determined using electrical and Hall measurements which require contacts to be made to the doped surface. It is also important to note that the carrier concentration itself is not a linear function of dopant concentration.

Since the Raman spectrum is sensitive to the interaction of dopants with the electronic continuum, it is in fact the carrier concentration, rather than the actual dopant concentration, to which the Raman spectrum is the most sensitive. Further complicating the picture is the fact that the morphology, growth rate and crystallite size are all sensitive to the amount of dopant in the gas mixture. The aforementioned factors conspire to make the interpretation of the Raman spectrum of doped diamond difficult, especially because it is in fact rare to find studies which have measured R, N_{dopant} and p (or n) all on the same films which have been used for the Raman studies. Nevertheless, quite some progress has been made, and some important insights gleaned from Raman studies, especially for boron-doped diamond.

(i) *Boron doping: the Fano effect*

Many authors (Gheeraert *et al*. 1993; Locher *et al*. 1995; Liao *et al*. 1997; Wang *et al*.; 2000; Einaga *et al*. 2001) have studied B doped polycrystalline CVD diamond films. With increasing hole concentration, an increasing asymmetry of the zero phonon line was observed. It was quickly realized that this asymmetry could be attributed to a Fano-type interference between the discrete zone-centre phonon and the continuum of electronic states induced by the presence of the dopant. As mentioned above, the incorporation of B on to {111} faces occurs much more readily than on to {100} surfaces. Ushizawa *et al*. (1998) studied this dependence by investigating the {100} and {111} facets of individual crystallites grown on silicon as a function of B/C in the gas phase. Parts (*a*) and (*b*) of figure 9 show the spectra for {100} and {111} facets, respectively. SIMS studies on homo-epitaxial films grown under similar conditions provided an estimate of the B concentration. It can be seen that for the same gas phase conditions the incorporation of B is much higher on {111} facets than on {100} facets.

The main features evident in figure 9 and from other papers are as follows.

(i) The zone-centre phonon line displays increasing asymmetry with increasing B concentration due to the Fano effect, with the minimum in the Raman scattering occurring on the high-energy side of the main Raman line. The strongest effect appears to occur when the doping level is *ca.* 2×10^{20} B cm^{-3}, which corresponds to the onset of metallic-type conductivity in the films (i.e. near-zero activation energy). This occurs when the density of dopants is sufficiently high that they form a continuous impurity band.

(ii) The Raman peak due to the silicon substrate decreases with increasing B concentration, as the doped material becomes more opaque at the wavelength of light used for the excitation.

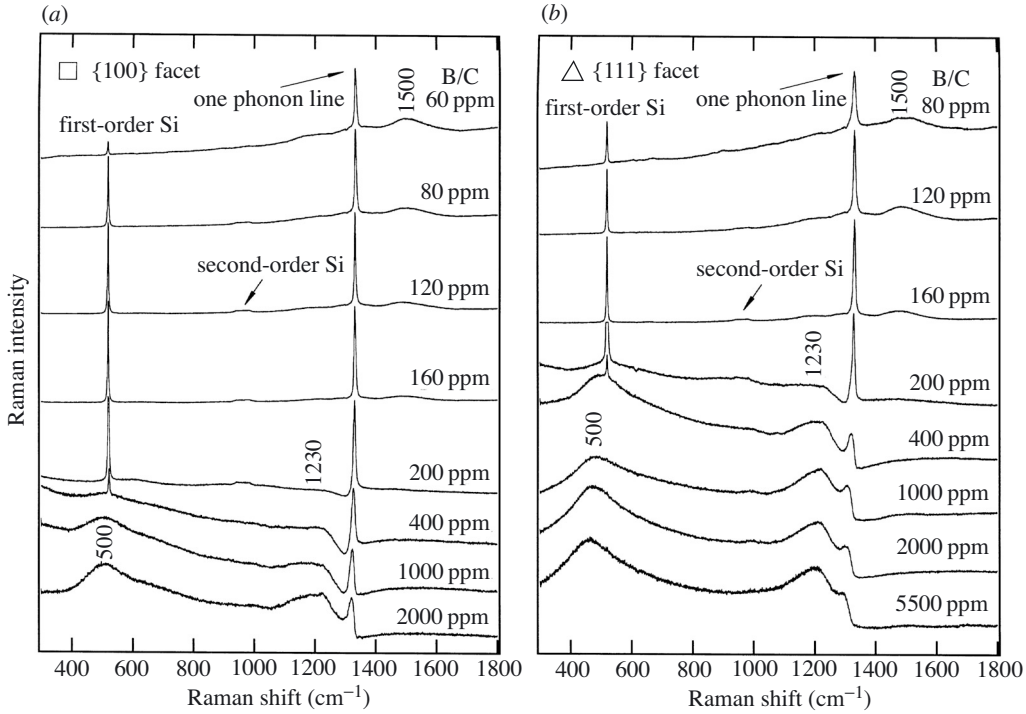

Figure 9. (*a*) Raman spectra of the {100} facets for B doped individual diamond crystals. B/C refers to the B/C in the gas phase. (*b*) Raman spectra of the {111} facets for B doped individual diamond crystals. B/C refers to the B/C in the gas phase. (After Ushizawa *et al.* (1998).)

(iii) New peaks appear at 500 cm^{-1} and 1230 cm^{-1}. The origin of these is uncertain; however, it is worth noting that these two band positions agree with the two maxima in the PDOS. They could therefore be connected with a relaxation of the wavevector selection rules. If so, they may well be associated with the actual boron incorporation in the lattice, rather than the hole concentration (see Bernard *et al.* 2004*a*). A recent suggestion (Bernard *et al.* 2004*b*) is that the 500 cm^{-1} band may originate from a pair of boron atoms.

Pruvost & Deneuville (2001) report a detailed analysis of the parameters extracted from the Fano line shape. They show that the Fano appears above a critical percolation threshold which corresponds to the onset of metallic conductivity. The trends are interpreted in terms of the relative Raman cross-sections for the continuum of electronic interband transitions compared with the cross-section for the phonon. It is clear that the Fano analysis is useful only for dopant levels close to, or exceeding, the percolation threshold for metallic conductivity (i.e. *ca.* 2×10^{20} B cm^{-3}). Unfortunately it cannot be used to estimate the more moderate B doping densities typical of those used for semiconducting films suitable for use in electronic devices such as p–n junctions.

Above the percolation threshold, the Fano parameters saturate. For extremely heavily doped films, it is difficult to discern the zone-centre phonon and the peaks at 500 and 1220 cm^{-1} dominate the spectrum. Bernard *et al.* (2004*a*) showed that in this region the 500 cm^{-1} peak could be fitted with a combination of Gaussian

and Lorentzian line shapes. The wavenumber, ω, of the Lorentzian component of the peak was found to obey the following relationship:

$$[\mathrm{B}]\ (\mathrm{in\ cm^{-3}}) = 8.44 \times 10^{30} \exp(-0.048\omega),$$

where ω is in $\mathrm{cm^{-1}}$ over a range of doping from 2×10^{20} to $1 \times 10^{22}\ \mathrm{B\ cm^{-3}}$, thus providing a contactless and non-destructive method for assessing doping levels in extremely heavily doped samples.

The temperature dependence of the Fano resonance in diamond was studied by Piccirillo *et al.* (2002). They reported that the Fano fitting parameters changed randomly with temperature around a mean value. No specific trend with temperature could be observed. However, later work (Connor *et al.* 2004) revealed that some of the scatter in the data was due to the fact that the Boron concentration was spatially inhomogeneous even at the micrometre scale, so that, as the sample drifted with increasing temperature, different regions were being probed. Reproducible trends could be observed when greater control over the exact location of the analysis spot on the sample was achieved using a metal mask on the sample surface to pinpoint the laser spot. The interpretation of the observed trends is not straightforward, although it seems that the coupling parameter appears to be the only quantity changing with temperature. One definite observation was that the temperature dependence of the Fano parameters derived from Raman measurements is quite different to that derived from IR measurements, leading to the conclusion that the nature of the interaction between discrete modes and the continuum of states is different in the two cases.

The Fano line shape and the presence of the 500 and 1230 $\mathrm{cm^{-1}}$ peaks also depend on the excitation energy. Locher *et al.* (1995) and later Wang *et al.* (2002) discerned the following trends with increasing excitation energy.

(i) The relative intensity of the electronic Raman scattering decreases, and the Fano-type interference becomes weak.

(ii) The observed position of the coupled zone-centre phonon moves to higher energies (recall that for undoped diamond there is no wavelength dependence of the zone-centre phonon energy). The position of the minimum in the spectrum moves from the high-wavenumber side to the low-wavenumber side.

(iii) The two peaks located at 500 and 1230 $\mathrm{cm^{-1}}$ become weak and cannot be detected at all when the Raman spectrum is excited by 244 nm light.

The reasons for these trends are not obvious, although they may be connected with the increased scattering cross-section for phonons ($\sigma \propto \omega_{\mathrm{L}}^4$), which does not apply to electronic Raman scattering.

(ii) *Doping with species other than boron*

It is well known that n-type doping remains challenging for diamond. Sulphur, phosphorus and lithium have all been tried, with quite some success in recent years in phosphorus doping of diamond ($E_{\mathrm{A}} = 600$ meV). Since the numbers of carriers remains comparatively low, one does not expect to observe a strong Fano-like resonance for n-type doping.

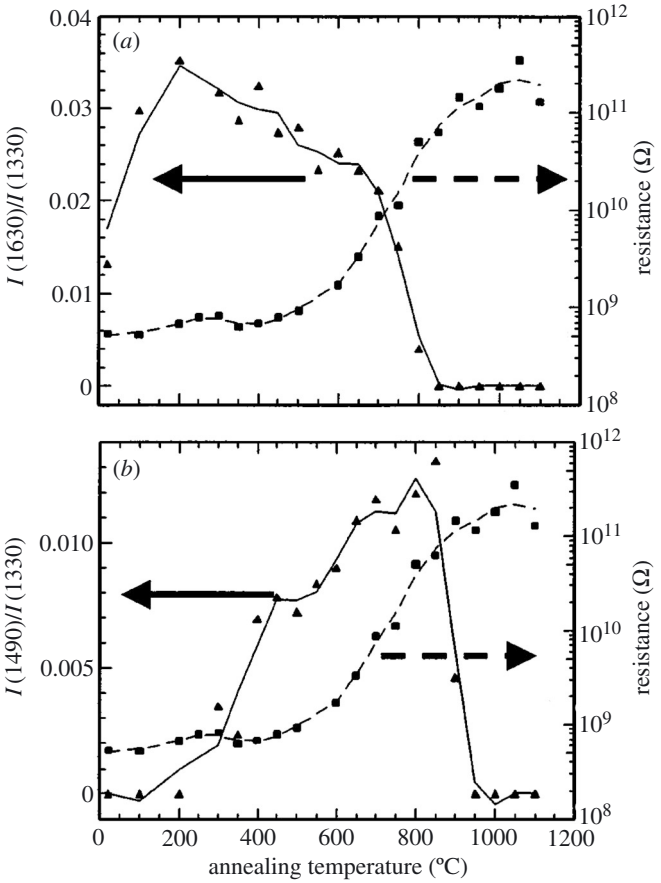

Figure 10. Normalized intensities of (*a*) interstitial and (*b*) vacancy related Raman peaks as a function of annealing temperature for B implanted type-IIa diamond. Also shown is the electrical resistance of the B implanted layer (right axis) (After Kalish *et al.* (2003).)

Of course, Raman is extensively used to monitor crystalline quality, stress and non-diamond incorporation into the films as a function of increasing dopant concentration (see, for example, Musale *et al.* 2002). To date, this sort of data, while useful, has not provided Raman parameters which can be correlated directly to dopant concentration.

Popovici *et al.* (1996) report the Raman spectra of Li doped diamond obtained by transmutation of ^{10}B into ^{7}Li. In addition to peaks at 1320 and 1500 cm^{-1}, they also observed a relatively sharp peak at 1629 cm^{-1}. However, in the transmutation from ^{10}B to ^{7}Li, 2.7 MeV of energy is released, which is imparted to the Li ion. Hence this situation is comparable with the damage created with light ions as described in § 2 *e*, with the 1620 cm^{-1} peak most probably due to the presence of split interstitials. In any case, the peak disappeared upon annealing at 1300 K.

Kalish *et al.* (2003) performed conductivity and Raman measurements on diamond implanted with sulphur. They addressed the question of whether there is evidence for electrically related conductivity in sulphur-ion-implanted diamond or whether the observed electrical activity could be simply related to the presence of residual ion-

implantation defects. Figure 10 shows the normalized intensities of the interstitial-related (a) and vacancy-related (b) defects as a function of annealing temperature for B implanted type-IIa diamond, compared with the electrical conductivity of the implanted layer. Although the data are shown for B implantations, very similar data were also obtained for C implantations. This figure shows that incomplete annealing (as evidenced by the presence of Raman peaks at 1490 and 1630 cm^{-1}) is concomitant with defect related electrical conductivity. Such data provide a baseline reference for the assessment of dopant related conductivity, particularly if the dopants have been introduced into the diamond lattice by ion implantation.

3. Conclusion

Raman spectroscopy has become an essential diagnostic tool for the diamond researcher. It is now well known that the typical Raman spectrum excited by a visible laser in the region 1000–2000 cm^{-1} contains basic information concerning the phase purity and crystalline perfection of the diamond material. But recent developments have shown that Raman spectroscopy can provide much more than this basic information. Surface-enhanced Raman spectroscopy has revealed the presence of new and unexpected structures on diamond surfaces. By combining information from different wavelength excitation, the sensitivity to sp^2 and sp^3 bonded phases can be tuned for particular applications. The Raman spectrum can be used to map stress and strain in crystallites on the micrometre scale, to remotely monitor the diamond surface temperature, and to monitor defect generation, annealing and electrical doping.

Future developments may lie in the combination of Raman microscopy with other analytical tools, especially those capable of improving the spatial resolution of the technique. Notable examples are the integration of Raman microscopes with near-field optical probes and most recently with scanning electron microscopes. These offer not only the possibility of spatial resolution of the order of 100 nm but also the capability of combining information from different scattering mechanisms (e.g. cathodoluminescence, photoluminescence and Raman) all on the same region of the sample.

References

Ager III, J. W. & Drory, M. D. 1993 Quantitative measurement of residual biaxial stress by Raman spectroscopy in diamond grown on a Ti alloy by chemical vapor deposition. *Phys. Rev.* B **48**, 2601.

Ager III, J. W., Veirs, D. K. & Rosenblatt, G. M. 1991 Spatially resolved Raman studies of diamond films grown by chemical vapor deposition. *Phys. Rev.* B **43**, 6491.

Anastassakis, E. 1999 Strain characterization of polycrystalline diamond and silicon systems. *J. Appl. Phys.* **86**, 249.

Asher, S. A. & Bormett, R. 2000 In *Raman scattering in materials science* (ed. W. H. Weber & R. Merlin), ch. 2, pp. 46–52. Springer.

Bergman, L. & Nemanich, R. J. 1995 Raman and photoluminescence analysis of stress state and impurity distribution in diamond thin films. *J. Appl. Phys.* **78**, 6709.

Bernard, M., Deneuville, A. & Muret, P. 2004*a* Non-destructive determination of the boron concentration of heavily doped metallic diamond thin films from Raman spectroscopy. *Diamond Relat. Mater.* **13**, 282.

Bernard, M., Baron, C. & Deneuville, A. 2004*b* About the origin of the low wave number structures of the Raman spectra of heavily boron doped diamond films. *Diamond Relat. Mater.* **13**, 896.

Bhargava S., Bist, H. D., Sahli, S., Aslam, M. & Tripathi, H. B. 1995 Diamond ploytypes in the chemical vapour deposited films. *Appl. Phys. Lett.* **67**, 1706.

Bormett, R. W., Asher, S. A., Witowski, R. E., Partlow, W. D., Lizewski, R. & Pettit, F. 1995 Ultraviolet Raman spectroscopy characterizes chemical vapor deposition diamond film growth and oxidation. *J. Appl. Phys.* **77**, 5916.

Campion, A. & Kambhanpati, P. 1998 Surface-enhanced Raman scattering. *Chem. Soc. Rev.* **27**, 241.

Connor, A. M., Piccirillo, C., Richards, D. R., Mainwood, A. & Davies, G. 2004 The temperature dependence of the Fano resonance in diamond. Presented at *Workshop on Surface and Bulk Defects in CVD Diamond Films IX*, 18–20 February 2004, Hasselt, Belgium.

Cui, J. B., Amtmann, K., Ristein, J. & Ley, L. 1998 Noncontact temperature measurements of diamond by Raman scattering spectroscopy. *J. Appl. Phys.* **83**, 7929.

Einaga, Y., Kim, G., Park, S. & Fujishima, A. 2001 A study of the crystalline growth of highly boron-doped CVD diamond: preparation of graded-morphology diamond thin films. *Diamond Relat. Mater.* **10**, 306.

Fauchet, P. M. & Campbell, I. H. 1988 Raman spectroscopy in low-dimensional semiconductors. *CRC Crit. Rev. Solid State Mater. Sci.* **14**, S79.

Ferrari, A. C. & Robertson, J. 2001 Origin of the 1150 cm^{-1} Raman mode in nanocrystalline diamond. *Phys. Rev.* B **63**, 121405.

Fleishman, M., Hendra, P. J. & McQuillan, A. J. 1974 Raman spectra of pyridine adsorbed at a silver electrode. *Chem. Phys. Lett.* **26**, 163.

Gardiner, D. J. & Graves, P. R. 1989 *Practical Raman spectroscopy*. Springer.

Gheeraert, E., Gonon, P., Deneuville, A., Abello, L. & Lucazeau, G. 1993 Effect of boron incorporation on the 'quality' of MPCVD diamond films. *Diamond Relat. Mater.* **2**, 742.

Grimsditch, M. H., Anastassakis, E. & Cardona, M. 1978 Effect of uniaxial stress on the zone center optical phonon of diamond. *Phys. Rev.* B **18**, 901.

Harris, S., Weiner, A. M., Nugent, K. W. & Prawer, S. 1996 Diamond film quality: effects of gas phase concentrations on the Raman spectra. *J. Appl. Phys.* **80**, 2187.

Huang, B. R., Chen, K. H. & Ke, W. Z. 2000 Surface-enhanced Raman analysis of diamond films using different metals. *Mater. Lett.* **42**, 162.

Jamieson, D. N., Prawer, S., Nugent, K. W. & Dooley, S. P. 1995 Cross sectional Raman microscopy of MeV implanted diamond. *Nucl. Instrum. Meth. Phys. Res.* B **106**, 641–645.

Kalish, R., Uzan-Saguy, C., Walker, R. & Prawer, S. 2003 Electrically active sulfur-defect complexes in sulfur implanted diamond. *J. Appl. Phys.* **94**, 3923.

Knight, D. S. & White, W. B. 1989 Characterization of diamond films by Raman spectroscopy. *J. Mater. Res.* **4**, 385.

Knight, D. S., Weimer, D., Pilione, L. & White, W. B. 1990 Surface-enhanced Raman spectroscopy of chemical vapor deposited diamond films. *Appl. Phys. Lett.* **56**, 1320.

Kunc, K., Lao, I. & Syassen, K. 2003 Equation of state and phonon frequency calculations of diamond at high pressures. *Phys. Rev.* B **68**, 094107.

Laikhtman, A. & Hoffman, A. 1997 Laser power effects on the Raman spectrum of isolated diamond chemical vapor deposition particles. *J. Appl. Phys.* **82**, 243.

Leeds, S. M., Davis, T. J., May, P. W., Pickard, C. D. O. & Ashfold, M. N. R. 1998 Use of different excitation wavelengths for the analysis of CVD diamond by laser Raman spectroscopy. *Diamond Relat. Mater.* **7**, 233.

LeGrice, Y. M., Nemanich, R. J., Glass, J. T., Lee, Y. H., Rudder, R. A. & Markunas, R. J. 1990 In *Diamond, Silicon Carbide and Related Wide-Bandgap Semiconductors. Proc. Symp. Materials Research Society* (ed. J. T. Glass), vol. 162, pp. 219. Warrendale, PA: Materials Research Society.

Liao, X. Z., Zhang, R. J., Lee, C. S., Tong Lee, S. & Lam, Y. W. 1997 The influence of boron doping on the structure and characteristics of diamond thin films. *Diamond Relat. Mater.* **6**, 521.

Liu, M. S., Bursill, L. A., Prawer, S. & Beserman, R. 2000 Temperature dependence of the first-order Raman phonon line of diamond. *Phys. Rev.* B **61**, 3391.

Locher, R., Wagner, J., Fuchs, F., Maier, M., Gonon, P. & Koidl, P. 1995 Optical and electrical characterization of boron-doped diamond films. *Diamond Relat. Mater.* **4**, 678.

Loh, M. H. & Cappelli, M. A. 1993 Supersonic DC-arcjet synthesis of diamond. *Diamond Relat. Mater.* **2**, 454.

López-Ríos, T. 1996 Diamond films studied by surface-enhanced Raman scattering. *Diamond Relat. Mater.* **5**, 608.

López-Ríos, T., Sandré, E., Leclercq, S. & Sauvain, E. 1996 Polyacetylene in diamond films evidenced by surface enhanced Raman scattering. *Phys. Rev. Lett.* **76**, 4935.

Louden, R. 1964 The Raman effect in crystals. *Adv. Phys.* **13**, 423.

Musale, D. V., Sainkar, S. R. & Kshirsagar, S. T. 2002 Raman, photoluminescence and morphological studies of Si- and N-doped diamond films grown on Si(100) substrate by hot-filament chemical vapor deposition technique. *Diamond Relat. Mater.* **11**, 75.

Nemanich, R. J., Solin, S. A. & Martin, R. M. 1981 Light scattering study of boron nitride microcrystals. *Phys. Rev.* B **23**, 6348.

Nugent, K. W. & Prawer, S. 1998 Confocal Raman strain mapping of isolated single CVD diamond crystals. *Diamond Relat. Mater.* **7**, 215.

Occelli, F., Loubeyre, P. & Letoullec, R. 2003 Properties of diamond under hydrostatic pressure up to 140 GPa. *Nat. Mater.* **2**, 151.

Okada, K., Komatsu, S., Ishigaki, T., Matsumoto, S. & Moriyoshi, Y. 1992 Evaluation of the surface structure of diamond films prepared in a combustion flame by surface-enhanced Raman scattering. *Appl. Phys. Lett.* **60**, 959.

Orwa, J. O., Nugent, K. W., Jamieson, D. N. & Prawer, S. 2000 Raman investigation of damage caused by deep ion implantation in diamond. *Phys. Rev.* B **62**, 5461.

Pfeiffer, R., Kuzmany, H., Salk, N. & Gunther, B. 2003 Evidence for trans-polyacetylene in nanocrystalline diamond films from H–D isotropic substitution experiments. *Appl. Phys. Lett.* **82**, 4149.

Piccirillo, C., Mainwood, A., Davies, G., Penchina, C. M., Tajani, A. & Bernard, M. 2002 The temperature dependence of the infrared absorption and Raman spectra due to boron in diamond. *Physica Status Solidi* A **193**, 529.

Popovici, G. (and 14 others) 1996 Properties of Li doped diamond films, obtained by transmutation of ^{10}B into ^{7}Li. *Diamond Relat. Mater.* **5**, 761.

Prawer, S., Hoffman, A., Stuart, S. A., Manory, R., Weiser, P., Lim, C., Long, C. & Ninio, F. 1991 Correlation between crystalline perfection and film purity for chemically vapor deposited diamond thin films grown on fused quartz substrates. *J. Appl. Phys.* **69**, 6625.

Prawer, S., Nugent, K. W. & Weiser, P. S. 1994 Polarized Raman spectroscopy of chemically vapor deposited diamond films. *Appl. Phys. Lett.* **65**, 2248.

Prawer, S., Nugent, K. W. & Jamieson, D. N. 1998 The Raman spectrum of amorphous diamond. *Diamond Relat. Mater.* **7**, 106.

Prawer, S., Nugent, K. W., Jamieson, D. N., Orwa, J. O., Bursill, L. A. & Peng, J. L. 2000 The Raman spectrum of nanocrystalline diamond. *Chem. Phys. Lett.* **332**, 93–97.

Prawer, S., Rosenblum, I., Orwa, J. O. & Adler, J. 2004 Identification of the point defects in diamond as measured by Raman spectroscopy: comparison between experiment and computation. *Chem. Phys. Lett.* **390**, 458–461.

Pruvost, F. & Deneuville, A. 2001 Analysis of the Fano in diamond. *Diamond Relat. Mater.* **10**, 531.

Richter, H., Wang, Z. P. & Ley, L. 1981 The one phonon Raman spectrum in microcrystalline silicon. *Solid State Commun.* **39**, 625.

Roy, D., Barber, Z. H. & Clyne, T. W. 2002*a* Ag nanoparticle induced surface enhanced Raman spectroscopy of chemical vapor deposition diamond thin films prepared by hot filament chemical vapor deposition. *J. Appl. Phys.* **91**, 6085.

Roy, M., George, V. C., Dua, A. K., Raj, P., Schulze, S., Tenne, D. A., Salvan, G. & Zahn, D. R. T. 2002*b* Detection of nanophase at the surface of HFCVD grown diamond films using surface enhanced Raman spectroscopic technique. *Diamond Relat. Mater.* **11**, 1858.

Sands, H. S., Demangeot, F., Bonera, E., Webster, S., Bennett, R., Hayward, I. P., Marchi, F., Smith, D. A. & Batchelder, D. N. 2002 Development of a combined confocal and scanning near-field Raman microscope for deep UV laser excitation. *J. Raman Spectrosc.* **33**, 730.

Schiferl, D., Nicol, M., Zaug, J. M., Sharma, S. K., Cooney, T. F., Wang, S.-Y., Anthony, T. R. & Fleischer, J. F. 1997 The diamond $^{13}C/^{12}C$ isotope Raman pressure sensor system for high-temperature/pressure diamond-anvil cells with reactive samples. *J. Appl. Phys.* **82**, 3256.

Stuart, S. A. 1993 The growth and characterization of chemical vapour deposited diamonds on tungsten wire tips. PhD thesis, RMIT University.

Stuart, S. A., Prawer, S. & Weiser, P. S. 1993*a* Growth-sector dependence of fine structure in the first-order Raman diamond line from large isolated chemical-vapor-deposited diamond crystals. *Appl. Phys. Lett.* **62**, 1227.

Stuart, S. A., Prawer, S. & Weiser, P. S. 1993*b* Variation of the raman diamond line shape with crystallographic orientation of isolated chemical-vapour-deposited diamond crystals. *Diamond Relat. Mater.* **2**, 753.

Sun, Z., Shi, J. R., Tay, B. K. & Lau, S. P. 2000 UV Raman characteristics of nanocrystalline diamond films with different grain size. *Diamond Relat. Mater.* **9**, 1979.

Tarutani, M., Shimato, Y., Takai, Y. & Shimizu, R. 1995 Cross-sectional transmission electron microscopy study of isolated diamond particles grown on a mirror-polished Si substrate. *Appl. Phys. Lett.* **67**, 632.

Ushizawa, K., Watanabe, K., Ando, T., Sakaguchi, I., Nishitani-Gamo, M., Sato, Y. & Kanda, H. 1998 Boron concentration dependence of Raman spectra on {100} and {111} facets of B-doped CVD diamond. *Diamond Relat. Mater.* **7**, 1719.

Ushizawa, K., Gamo, M. N., Kikuchi, Y., Sakagushi, I., Sato, Y. & Ando, T. 1999 Surface-enhanced Raman spectroscopic study of hydrogen and deuterium chemisorption on diamond (111) and (100) surfaces. *Phys. Rev.* B **60**, R5165.

Wagner, J., Wild, C. & Koidl, P. 1991 Resonance effects in Raman scattering from polycrystalline diamond films. *Appl. Phys. Lett.* **59**, 779.

Wang, Y., Li, H., Xiong, Y., Zhang, S., Lin, Z. & Feng, K. 2000 Micro-Raman scattering and photoluminescence study of boron-doped diamond films. *Diamond Relat. Mater.* **9**, 1708.

Wang, Y. G., Lau, S. P., Tay, B. K. & Zhang, X. H. 2002 Resonant Raman scattering studies of Fano-type interference in boron doped diamond. *J. Appl. Phys.* **92**, 7253.

Windischmann, H. & Gray, K. J. 1995 Stress measurement of CVD diamond films. *Diamond Relat. Mater.* **4**, 837.

Zaitsev, A. M. 2001 *Optical properties of diamond*. Springer.

Zuiker, C. D., Kraus, A. R., Gruen, D. M., Carlisle, J. A., Terminello, L. J., Asher, S. A. & Bormett, R. W. 1996 Applications of synchrotron radiation techniques to materials science. III. In *Proc. Symp. Materials Research Society*, p. 211. Warrendale, PA: Materials Research Society.